Novel Schiff Bases of Pyrrole: Synthesis, Experimental and Theoretical Characterizations, Fluorescent Properties and Molecular Docking

Khashi, Maryam*[+]

Young Researchers and Elite Club, Mashhad Branch, Islamic Azad University, Mashhad, I.R. IRAN

Beyramabadi, Safar Ali; Gharib, Azar

Department of Chemistry, Mashhad Branch, Islamic Azad University, Mashhad, Iran, I.R. IRAN

ABSTRACT: *Some new Schiff-base compounds based on pyrrole were synthesized by the reaction of 2-amino-1-methyl-4,5-diphenyl-1H-pyrrole-3-carbonitrile (**1**) with aromatic aldehydes (**2a-2e**) in ethanol/acetic acid at room temperature. The structures of the Schiff bases were characterized by full spectral data. The fluorescence emission intensity of the Schiff bases has been measured in different polar solvents (protic and aprotic) at different temperatures and also pHs. Among the products of this reaction, 2-[(2-hydroxy-benzylidene)-amino]-1-methyl-4,5-diphenyl-1H-3-carbonitrile (**3a**) exhibited good results. The molecular docking studies on all Schiff bases revealed that the compound **3a** forms a stable complex with polo-like kinase1 as a target and gives a binding affinity value of -8.9 kcal/mol. According to the obtained results, the DFT calculations carried out on **3a** by using B3LYP/6-31+G(d,p) level of theory which the theoretical data were in good agreement with the experimental data. Furthermore, the NBO analysis showed the electron transfers correctly.*

KEYWORDS: *Schiff-base; DFT; NBO; Fluorescent properties; Tautomerism; Molecular docking.*

INTRODUCTION

Schiff-base ligands are a significant class of organic compounds due to their structure and [1, 2] pharmaceutical activities such as antibacterial, anticancer, anti tumor and anti-inflammatory [3-7]. These compounds have a large number of applications specially in the field of inorganic chemistry as a ligand for complexation [8-12], in biochemistry area as intermediate in the enzymatic reactions and also as a dye for detection of proteins [13-17]. In addition, because of fluorescence properties in the Schiff-base ligands and their complexes, they can be used as a selective fluorescent indicator for the detection of metals [18].

Chemistry of pyrrole and its derivatives have received considerable attention owing to their synthesis and biological activities [19, 20]. Pyrrole is one of the most important simple heterocycles, which has been found in the marine natural products, including dimeric structures such as nakamuric acid [21]. Moreover, the pyrrole based

* *To whom correspondence should be addressed.*

+ E-mail: maryamkhashi@mshdiau.ac.ir ; maryamkhashii@gmail.com

1021-9986/2018/6/59-72 14/$/6.04

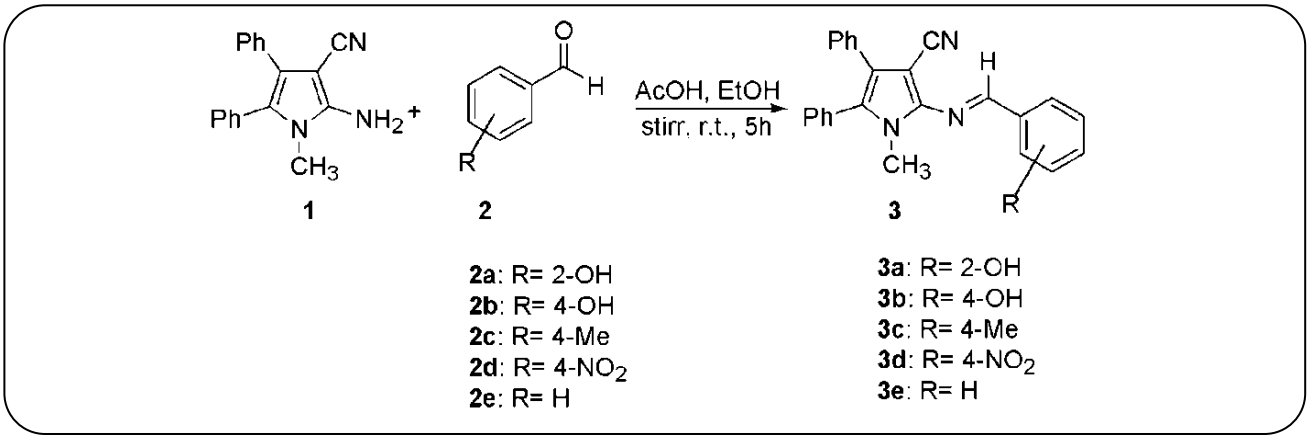

Scheme 1: Synthesis of the Schiff bases

Schiff bases and their complexes have been very important duo to their applications for example electrochromic [22] photovoltaic [23] and also they have used as fluorescent and colorimetric chemosensors [24, 25].

On the other hand, materials containing electroluminescent have widely investigated experimentally and theoretically [26-29]. Also, Schiff-base ligands and their complexes are an important class of organic and inorganic compounds because of their fluorescent properties [30-32].

Furthermore, the theoretical evaluation of pyrrole derivatives structure has been shown the good results. Also, the study of biological structures and interaction with the pyrrole derivatives has predicted considerable results [33, 34]. Hence, these findings promoted us to synthesis some new Schiff bases of pyrrole (**3a-3e**) *via* the reaction of 2-amino-1-methyl-4,5-diphenyl-3-carbonitrile (**1**) with aromatic aldehydes (**2a-2e**) in the acidic solution of ethanol at room temperature (Scheme 1). Also, we have evaluated the fluorescence properties, molecular docking for all compounds. Because of the structural similarity between products, the DFT calculations carried out for **3a** selectivity.

The pyrrole derivatives have shown many significant biological properties such as anticancer and inhibitor [35-37]. The Polo-Like Kinas1 (PLK1) is an enzyme, which is considered as a target for cancer drugs. The PLK1 is considered as a proto-oncogene, whose over expression is often observed in tumor cells. Many cancers are dependent on this inhibitor [38, 39]. Hence, the interaction of the **3a-3e** compounds with PLK1 has been explored theoretically.

EXPERIMENTAL SECTION

Material and physical sciences

All anhydrous solvents and chemicals were obtained from Sigma Aldrich without purification. ^{1}H NMR (300 MHz) and ^{13}C NMR (75 MHz) spectra were recorded on a Bruker spectrometer in $CDCl_3$ solution. Mass spectra were obtained using a Thermo Finnigan LCQ DECA XP MAX mass spectrometer. Elemental analysis was performed on a Thermo Finnigan Flash EA microanalyzer. Fluorescence emission spectra were recorded on a Varian Cary Eclipse (Australia) equipped with Cary Eclipse software by Quartz cell 1 cm for fluorescence. FT-IR spectrum was recorded on a Bruker Tensor 27 spectrometer (KBr discs, 4000-400 cm^{-1}). Melting point (mp) was recorded on a Stuart SMP3 melting point apparatus.

General procedure for the synthesis of Schiff-bases 3a-3e

2-amino-1-methyl -4,5- diphenyl- 1*H*-pyrrole -3-carbonitrile (**1**) (1mmol) and aromatic aldehydes (**2a-2e**) (1mmol) were added to a solution of ethanol (3 mL) in acetic acid (0.03 mL). The reaction mixture was stirred at room temperature for 5h. The obtained yellow solid was filtered, washed with ethanol and dried in 100 °C.

Spectral data

2-[(2-hydroxy-benzylidene)-amino]-1-methyl-4,5-diphenyl- 1H-3-carbonitrile (3a)

^{1}H NMR (300 MHz, $CDCl_3$): δ 3.59 (s, 3H, N−CH_3), 7.01-7.07 (m, 2H, arom-H), 7.25-7.28 (m, 7H, arom-H), 7.39-7.49 (m, 4H, arom-H), 7.54-7.57 (m, 1H, arom-H), 9.36 (s, 1H, N=CH) ppm, 12.33 (s, 1H, phenolic OH);

^{13}C NMR (75 MHz, $CDCl_3$): δ 31.65 (N−CH_3), 79.45 (CN), 117.20, 117.53, 120.17, 121.21, 124.08, 127.47, 128.86 (2C), 129.07, 129.16 (2C), 129.38 (2C), 129.84, 130.37, 130.76, 131.35 (2C) (phenyl rings), 132.92, 134.74 (pyrrole ring), 145.52 (C=N), 159.92 (N−C=N, pyrrole ring), 160.00 (C−OH); Mass (APCI): *m/z* 378.11 (MH^+, 100%) (377.15 calcd. for $C_{25}H_{19}N_3O$); Anal. calcd. for $C_{25}H_{19}N_3O$: C, 79.55; H, 5.07; N, 11.13; found: C, 79.30; H, 5.00; N, 11.45; m.p.: 213 °C; yield: 85 %.

2-[(4-hydroxy-benzylidene)-amino]-1-methyl-4,5-diphenyl-1H-3-carbonitrile (3b)

^{1}H NMR (300 MHz, $CDCl_3$): δ 3.68 (s, 3H, CH_3), 7.12 (m, 2H, arom-H), 7.20-7.36 (m, 10H, arom-H), 7.81 (d, 2H, *J*= 8.7 Hz, arom-H), 9.20 (s, 1H, CH) ppm, 12.30 (s, 1H, phenolic OH); ^{13}C NMR (75 MHz, $CDCl_3$): δ 31.68 (CH_3), 79.31 (CN), 117.23, 120.00, 123.98, 127.50, 128.22, 128.78 (2C), 129.10, 129.21 (2C), 129.84 (2C), 130.45 (2C), 131.02 (2C), 131.43 (2C) (phenyl ring), 133.12, 134.80 (pyrrole ring), 145.32 (C=N), 158.61 (N−C=N, pyrrole ring), 160.10 (C−OH); Mass (APCI): *m/z* 378.10 (MH^+, 100%) (377.15 calcd. for $C_{25}H_{19}N_3O$); Anal. calcd. for $C_{25}H_{19}N_3O$: C, 79.55; H, 5.07; N, 11.13; found: C, 79.43; H, 5.10; N, 11.22; m.p.: 235 °C; yield: 83 %.

2-[(4-methyl-benzylidene)-amino]-1-methyl-4,5-diphenyl-1H-3-carbonitrile (3c)

^{1}H NMR (300 MHz, $CDCl_3$): δ 2.83 (s, 3H, CH_3), 3.69 (s, 3H, N−CH_3), 7.31-7.42 (m, 6H, arom-H), 7.43-7.45 (m, 4H, arom-H), 7.68 (d, 2H, *J*= 8.00 Hz, arom-H), 7.92 (d, 2H, *J*= 8.00 Hz, arom-H), 9.17 (s, 1H, CH) ppm; ^{13}C NMR (75 MHz, $CDCl_3$): δ 27.43 (CH_3), 31.66 (N−CH_3), 79.29 (CN), 117.13, 117.59, 120.03, 120.49, 121.07, 121.59, 123. 44, 123.93 (2C), 126.69 (2C), 128.17 (2C), 128.32, 128.56, 129.31, 130.10 (2C), 131.09 (2C) (phenyl rings), 145.43 (C=N), 158.71 (N−C=N, pyrrole ring); Mass (APCI): *m/z* 376.20 (MH^+, 100%) (375.17 calcd. for $C_{26}H_{21}N_3$); Anal. calcd. for $C_{26}H_{21}N_3$: C, 83.17; H, 5.64; N, 11.19; found: C, 83.08; H, 5.73; N, 11.20; m.p.: 241 °C; yield: 93 %.

2-[(4-nitro-benzylidene)-amino]-1-methyl-4,5-diphenyl-1H-3-carbonitrile (3d)

^{1}H NMR (300 MHz, $CDCl_3$): δ 3.70 (s, 3H, CH_3), 7.28-7.30 (m, 7H, arom-H), 7.41-7.44 (m, 3H, arom-H), 8.15 (d, 2H, *J*= 8.40 Hz, arom-H), 8.36 (d, 2H, *J*= 8.40 Hz, arom-H), 9.38 (s, 1H, CH) ppm; ^{13}C NMR (75 MHz, $CDCl_3$): δ 31.70 (N−CH_3), 79.47 (CN), 117.22, 117.53, 120.20, 121.23, 124.10, 127.50, 128.35, 128.89 (2C), 129.12 (2C), 129.20 (2C), 129.41, 129.91, 130.15 (2C), 130.22, 131.41 (2C) (phenyl rings), 145.23 (C=N), 160.00 (N−C=N, pyrrole ring); Mass (APCI): *m/z* 407.21 (MH^+, 100%) (406.14 calcd. for $C_{25}H_{18}N_4O_2$); Anal. calcd. for $C_{25}H_{18}N_4O_2$: C, 73.88; H, 4.46; N, 13.78; found: C, 73.79; H, 4.27; N, 14.06; m.p.: 249 °C; yield: 90 %.

2-[(benzylidene)-amino]-1-methyl-4,5-diphenyl-1H-3-carbonitrile (3e)

^{1}H NMR (300 MHz, $CDCl_3$): δ 3.72 (s, 3H, N−CH_3), 7.10-7.27 (m, 15H, arom-H), 9.23 (s, 1H, CH) ppm; ^{13}C NMR (75 MHz, $CDCl_3$): δ 31.79 (N−CH_3), 79.43 (CN), 116.90, 117.20, 117.50, 120.10, 120.21, 121.21, 122.00, 122.95 (2C), 125.47 (2C), 126.64 (2C), 127.10, 127.33, 128.00, 128.51 (2C), 128.71, (2C) (phenyl rings), 140.00 (C=N), 158.64 (N−C=N); Mass (APCI): *m/z* 362.23 (MH^+, 100%) (361.16 calcd. for $C_{25}H_{19}N_3$); Anal. calcd. for $C_{25}H_{19}N_3$: C, 83.07; H, 5.30; N, 11.63; found: C, 82.81; H, 5.23; N, 11.96; m.p.: 230 °C; yield: 98 %.

RESULTS AND DISCUSSION

Experimental spectral analysis

The structures of new Schiff-bases **3a-3e** were deduced from their spectral data. For example, the ^{1}H NMR spectrum of **3a** in $CDCl_3$ did not show the $–NH_2$ signal belonging to the precursor **1**, but instead showed a sharp signal at 12.33 ppm for a –OH group (Fig. 1). The FT-IR spectrum was devoid of the $–NH_2$ absorption peaks at 3427 and 3327cm^{-1}, which shows the inclusion of the azomethine bond in the process. The –OH group absorption observed as a broad peak at 3425 cm^{-1} (Fig. 2). Also, ^{13}C NMR showed 21 carbons for this structure.

Fluorescence spectroscopy

The fluorescent properties of compounds **3a-3e** were examined under different conditions such as different non-aqueous solvents, temperatures, and pHs. All measurements were done in 1 cm × 1 cm cuvette. The fluorescence emission spectra were recorded at an optimized concentration of 10^{-5} mol/lit in different solvents. The fluorescence excitation wavelengths were 230 and

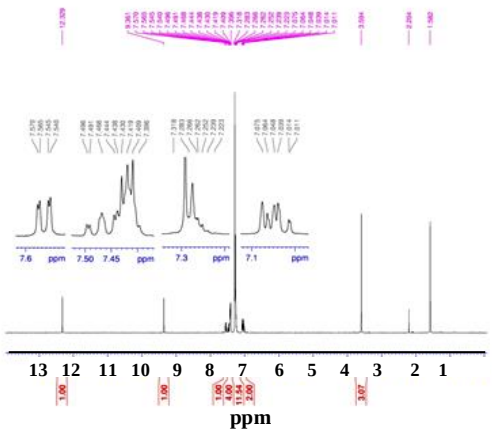

Fig. 1: The ^{1}H NMR spectrum of compound 3a.

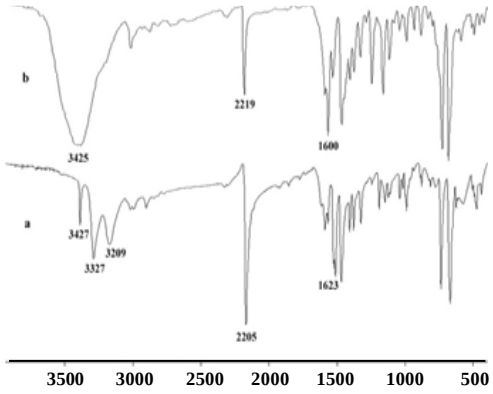

Fig. 2: The FT-IR spectra of a: 1 and b: 3a.

260 nm, maximum emission wavelengths (λ_{flu}/nm) were between 400-600 nm in all conditions respectively.

Effect of temperature and pH changes in different solvents

The effect of different temperatures (15, 25, 35, 45 °C) and pHs (1.5, 3.5, 5.5, 7.5, 9.5) on the fluorescence emission intensity of the new Schiff-bases **3a-3e** have measured in two polar protic solvents such as ethanol and methanol and three polar aprotic solvents like N,N-dimethylformamide (DMF), dimethylsulfoxide (DMSO) and acetonitrile.

Among the compouds **3a-3e**, the **3a** species showed the flourescence emission spectrum in various conditions. As can be seen (Table 1), the fluorescence emission intensity has generally been decreased with increasing temperature for **3a**. This phenomenon can be explained by the non radiative processes related to the thermal agitation such as intermolecular vibrations, collisions with solvent molecules [40] and also deactivation processes such as external conversion in high temperature which increase the frequency of collision and Brownian phenomenon [40, 41]. At low temperatures, the solvents have more viscosity which increases the time for reorientation [42].

The results showed that among the polar protic solvents, methanol has the highest fluorescence emission intensity equals 95 a.u. at 15 °C (Fig. 3, A, Table 1). This distinct behavior of methanol can be explained by its molecular properties. Methanol is smaller than ethanol and its intractions with the molecular environment are strongly dominated by the polar hydroxyl group. Among the polar aprotic solvents, DMSO has been exhibited the highest fluorescence emission intensity equals 863 a.u. at 15 °C.

Some aromatic and heteroaromatic compounds have many mesomeric structures. These structures can be protonated in the acidic solutions and also deprotonated in the basic solutions. In these compounds, fluorescence emission intensity depends on the pH. On the other hand, suppressin can be observed in these conditions [43].

The existance of a –OH group as an electron donating moiety and a –CN group as an electron accepting moiety in **3a** species causes the Intramolecular Charge Transfer (ICT) from –OH to –CN (Scheme 2). The intramolecular charge transfer has an important rule in the fluorescence intensity specially in different pHs.

The results showed that the highest fluorescence emission intensity have occurred at pH = 7.5 for all solvents and as usual DMSO has the more amount of intensity equals 468 a.u. (Fig. 6, B).

Other compounds, according to the solubility showed the flourescence emission spectrum in some solvents (Fig. 4).

Molecular docking

High resolution crystal structure of PLK1 was downloaded from the RCSB protein data bank website with PDB ID: 4A4L and the molecular docking calculations were performed on Auto Dock-Vina software [44].

Table 1: Spectroscopic data for 3a at λ_{flu}/nm = 520

Temperature (°C)	Acetonitrile μ= 3.92 D Mw: 41.05 g/mol d: 0.786 g/mL	DMF μ= 3.86 D Mw: 73.10 g/mol d: 0.948 g/mL	DMSO μ= 3.96 D Mw: 78.13 g/mol d: 1.10 g/mL	Ethanol μ= 1.69 D Mw: 46.07 g/mol d: 0.79 g/mL	Methanol μ= 1.70 D Mw: 32.04 g/mol d: 0.79 g/mL
15	256	209	863	86	95
25	248	208	862	83	84
35	234	204	826	81	68
45	217	206	779	70	55
pH	Acetonitrile	DMF	DMSO	Ethanol	Methanol
1.5	135	167	276	86	96
3.5	227	232	413	88	104
5.5	226	240	449	106	135
7.5	246	245	468	146	185
9.5	199	222	452	109	122

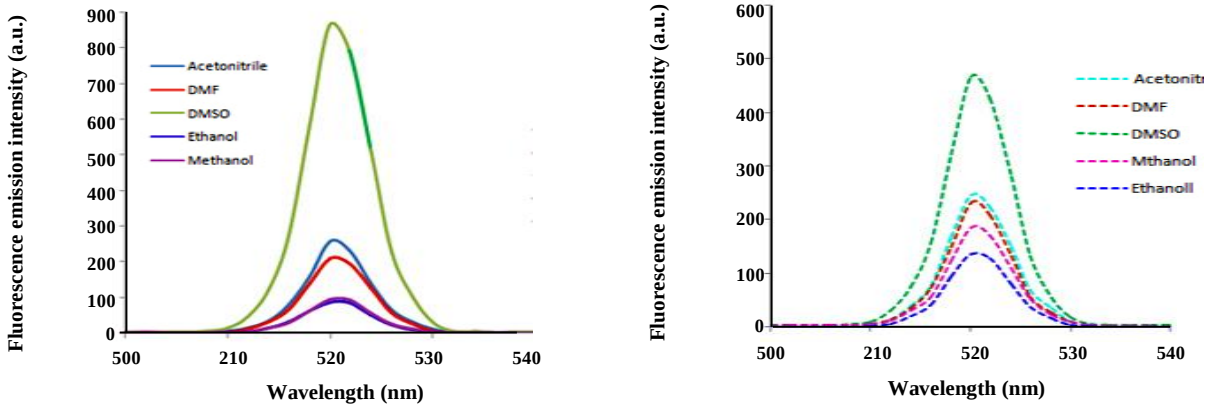

Fig. 3: The maximum fluorescence emission intensity for 3a species in different solvents, A: at 15 °C, B: pH = 7.5.

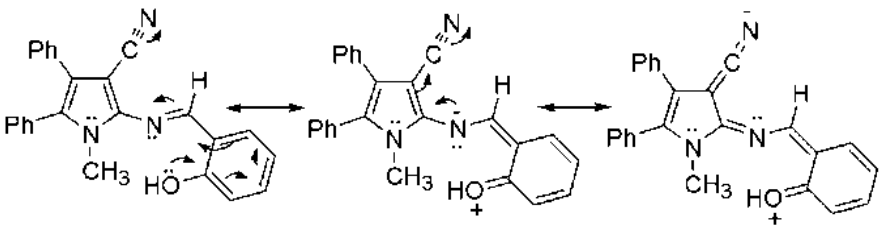

Scheme 2: Mesomeric structures of 3a.

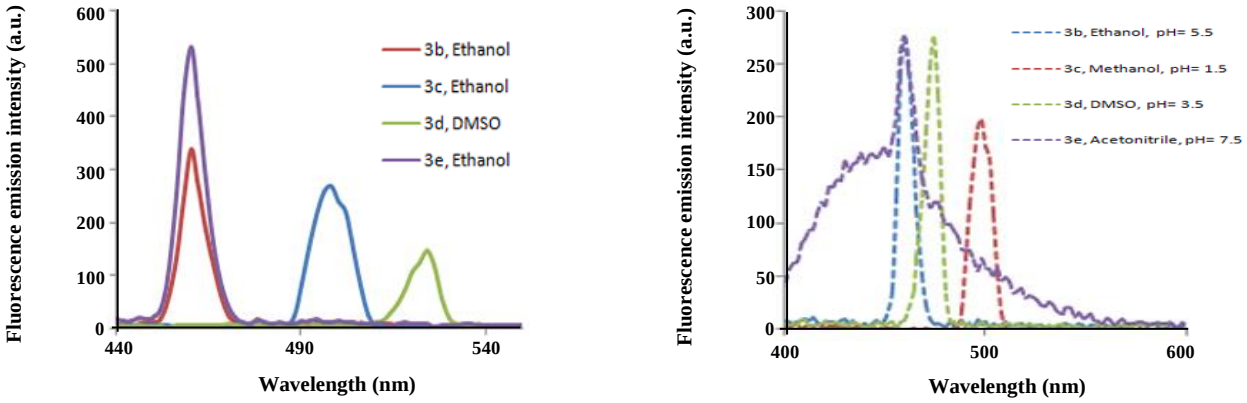

Fig. 4: The maximum fluorescence emission intensity for 3b-3e in different solvents, C: at different temperatures and D: at different pHs.

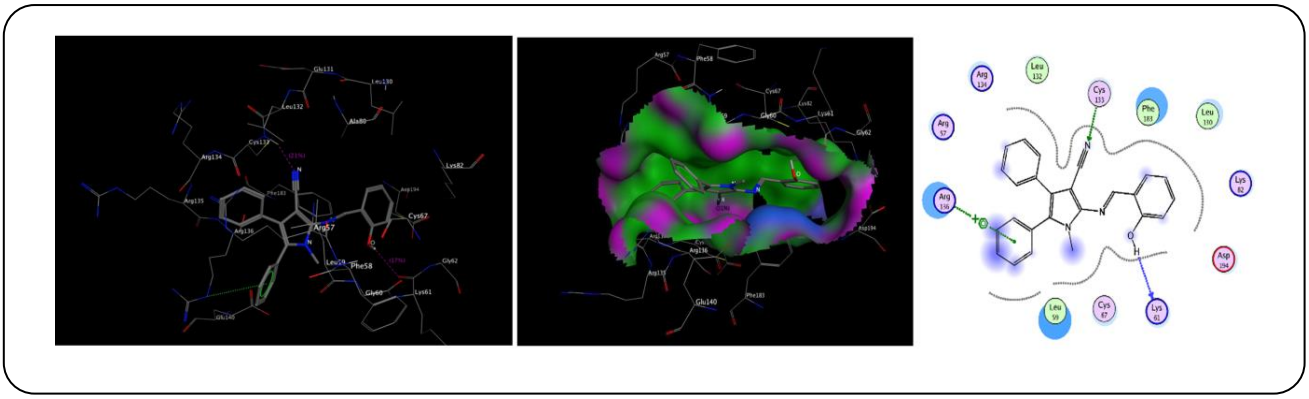

Fig. 5: The interactions of the ligand 3a with PLK1.

The docking studies have exhibited that among the Schiff bases; the docked ligand **3a** forms a stable complex with the PLK1 and gives a binding affinity value of -8.9 kcal/mol. As seen in Fig. 5, the Cys 133, Lys 61 and Arg 136 amino acids interact with the **3a** ligand. The root-mean-square deviation (RMSD) values of the **3a** ligand are given in Table 2. The obtained results show that the **3a** ligand might be active as an inhibitor or anticancer drug.

COMPUTATIONAL DETAILS

All of the calculations were performed using the Gaussian 03 software package [45]. The B3LYP functional and the 6-31+G(d,p) basis set were used. First, all geometries were fully optimized. Optimized geometries were confirmed to have no imaginary frequency, except for Transition State (TS) which have only one imaginary frequency of the *Hessian* [46]. The ^{1}H-NMR chemical shifts were predicted with respect to tetramethylsilane (TMS), where the GIAO method was employed [47]. The geometric structures were visualized by employing the Chemcraft 1.7 program.

Geometry and tautomerism of the Schiff-bese 3a

In this work, the Schiff bases of a pyrrole derivative were newly synthesized. The optimized geometric parameters such as bond lengths and bond angles have been calculated for **3a**. The aforesaid Schiff base could exist as two possible tautomers, Enol and Keto. Geometries of two possible tautomers are fully optimized in the methanolic solution. Their optimized geometries with the labeling of their atoms are shown in Fig. 6. Also, the Enol-Keto tautomerization of the Schiff base has been investigated in details. The transition state of the Enol-Keto tautomerization was named as **TS1**. Optimized geometry of the **TS1** is shown in Fig. 7. Selected-structural

Table 2: The binding affinity values of different poses of the Schiff base 3a.

Mode	Binding Affinity (kcal/mol)	RMSD lower bond	RMSD upper bond
0	-8.9	0	0
1	-8.4	4.544	2.693
2	-7.6	7.969	4.303
3	-7.5	32.88	30.954
4	-7.2	32.66	30.069
5	-7.1	13.3	8.04
6	-6.9	31.927	29.513
7	-6.8	28.018	23.927
8	-6.8	30.874	27.068

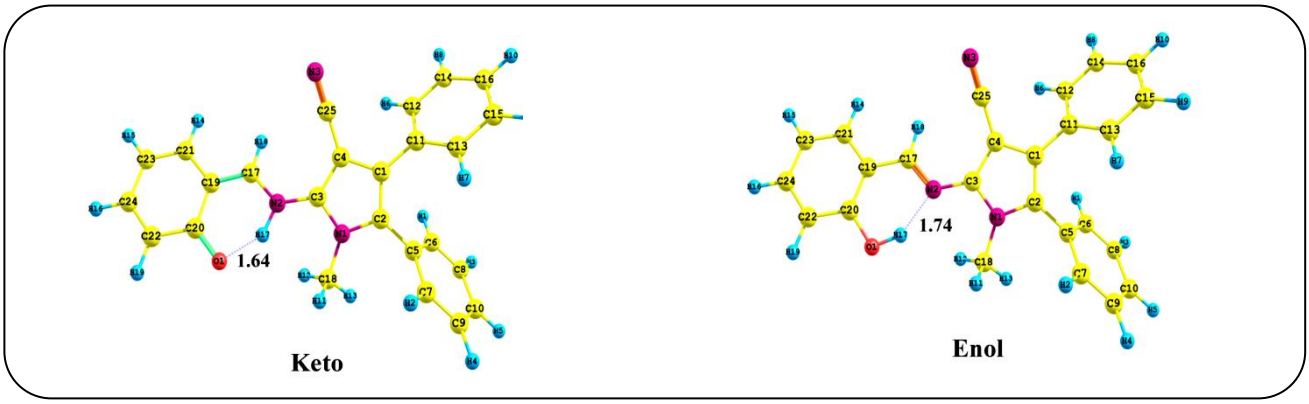

Fig. 6: Optimized geometries for the Enol and Keto tautomers of the Schiff base 3a.

parameters of the investigated species are gathered in Table 3. The calculated-structural parameters are good in agreement with the data reported for the similar compounds [48-51]. In the optimized geometry of the Enol tautomer, the proton of the phenolic –OH group (H17) is engaged in the hydrogen-bond interaction with the N2 imine nitrogen. The O1H17…N2 distance is 1.74 Å. This intramolecular H-bond forms a six-membered cycle. In comparison with the Enol tautomer, in the Keto tautomer, the H17 proton transfers from O1 atom of the phenolic –OH group to N2 atom of the azomethine nitrogen *via* an Intermolecular Proton Transfer (IPT).

Going from the Enol to the Keto tautomer, some structural parameters have been changed, important of which are: The N2… H17 and O1…H17 distances are 1.74 and 0.99 Å in the Enol tautomer, respectively, which change to 1.00 and 1.64 in the Keto tautomer, respectively. These parameters are 1.16 and 1.35 Å in the optimized geometry of the **TS1** species. The C20-O1 bond length decreases form 1.35 to 1.28 Å, whereas the C17-N2 bond length enlarges from 1.30 to 1.33 Å. These bond lengths are 1.30 And 1.33 Å in the **TS1**, respectively. Since, in the optimized geometry of the **TS1** (Fig. 7), the formation of the N2-H17 and breaking of the O1-H17 bond is clear.

In methanol solution, the Enol tautomer is more stable than the Keto tautomer by 27.41 kJ.mol^{-1}. The activation energy of the Enol-Keto tautomerization is 28.56 kJ/mol in the methanol solution. Considering the equilibrium between the Enol and Keto tautomers, the value of the tautomeric equilibrium constant (K) is calculated by using

$$K = \exp\left(-\frac{\Delta G}{RT}\right) \quad (1)$$

Where ΔG, R, and T are the Gibbs free energy difference between the two tautomers, the gas constant and temperature, respectively. In the methanol solution,

Table 3: Selected structural parameters of the optimized geometry 3a.

Atoms	Bond length (Å)			Angle (°)				Dihedral angle (°)			
	Enol	Keto	TS1		Enol	Keto	TS1	Atoms	Enol	Keto	TS1
C3-N2	1.38	1.38	1.38	N2-C3-N1	118.7	120.0	119.5	N1-C3-N2-C17	-162.5	-159.3	-166.0
C17-N2	1.30	1.33	1.33	C3-N2-C17	27.8	26.0	126.8	C3-N2-C17-C19	-177.0	-176.4	-177.5
C17-C19	1.45	1.40	1.41	N2-C17-C19	121.9	121.0	119.3	N2-C17-C19-C21	-179.4	-180.0	-179.9
C19-C20	1.42	1.46	1.45	C17-C19-C21	119.3	119.8	120.9	N2-C17-C19-20	0.8	-0.1	0.2
C20-O1	1.35	1.28	1.30	C17-C19-C20	122.03	119.9	118.9	C17-C19-C20-O1	-0.3	-0.6	-0.6
O1-H17	0.99	1.64	1.35	C19-C20-O1	121.5	121.2	120.3	C19-C20-O1-H17	0.6	0.9	0.7
C3-C4	1.41	1.40	1.40	C20-O1-H17	107.3	103.4	103.2	C22-C20-O1-H17	-179.5	-179.3	-179.5
C4-C25	1.41	1.41	1.41	C22-C20-O1	118.6	122.2	122.2	N2-C3-N1-C18	7.2	6.6	6.2
C25-N3	1.17	1.17	1.17	C3-N1-C18	123.4	124.0	123.8	C4-C3-N1-C18	-175.2	-174.4	-174.8
C3-N1	1.37	1.37	1.37	C3-N1-C2	110.1	109.4	109.6	N1-C3-C4-C25	-174.2	-174.7	-175.2
C18-N1	1.46	1.46	1.46	C3-C4-C25	126.0	125.9	126.0	C3-C4-C25-N3	121.2	-0.4	4.9
C2-N1	1.39	1.39	1.39	C4-C25-N3	179.8	179.6	179.7	C3-C4-C1-C11	-177.7	-177.9	-178.0
C2-C5	1.48	1.48	1.48	C1-C4-C25	126.0	126.7	126.4	C4-C1-C11-C12	-48.7	-48.6	-48.7
C5-C7	1.41	1.41	1.41	C4-C1-C2	106.6	106.8	106.7	C4-C1-C2-C5	178.6	179.1	178.9
C5-C6	1.41	1.41	1.41	C1-C2-C5	129.2	129.5	129.3	C1-C2-C5-C7	124.1	123.8	123.3
C1-C11	1.48	1.48	1.48	C2-C1-C11	127.5	127.7	127.6	N1-C2-C5-C7	-57.3	-57.7	-58.2
C11-C12	1.41	1.41	1.41	C1-C11-C12	120.5	120.5	120.5	C5-C2-N1-C18	-3.9	-4.8	-4.2
C11-C13	1.41	1.41	1.41	C1-C11-C13	121.1	121.0	121.0	C11-C13-C5-C7	-150.2	-149.7	-150.1
N2-H17	1.74	1.00	1.16	C2-C5-C7	121.2	121.2	121.2	C5-C2-C1-C11	-3.8	-3.4	-3.4
				C2-C5-C6	120.1	120.1	120.0	C11-C1-C4-C25	-3.3	-3.2	-2.7

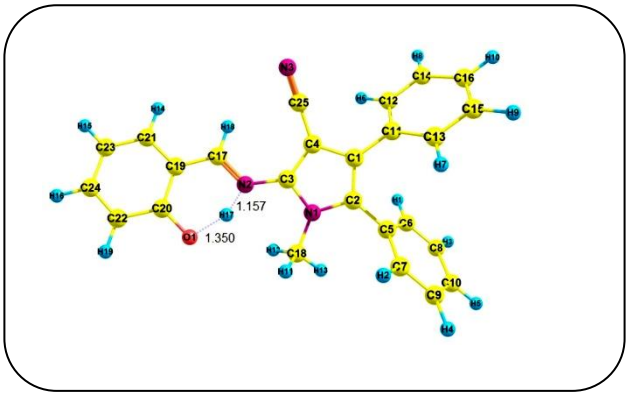

Fig. 7: The optimized geometry of TS1 for 3a

the calculated ΔG between two tautomers is 25.44 kJ/mol. By using the Eq. (1), amounts of the Keto tautomer in methanol solution of the titled Schiff base is predicted to be negligible.

In the optimized geometry of the Enol tautomer, the cyanide and methyl substituents are roughly in the same plane with the pyrrole ring. But, two phenyl substituents make dihedral angles of about 50° with the pyrrole ring. The azomethine group (C17-N2) is in the same plane with the benzene ring, while makes a dihedral angle of about 20° with the pyrrole ring. For example, the calculated C20-C19-C17-N2, C17-N2-C3-C4, and C17-N2-C3-N1 dihedral angles are 0.8, 20.7 and -162.5°, respectively.

Theoretical NMR spectral analysis

Theoretical assignment of the spectra is a quantitative framework for identification of the chemical compounds. The DFT computed ^{1}H NMR and ^{13}C NMR chemical shifts (δ) for the Enol tautomer of the titled compound are

Table 4: Experimental and DFT computed ^{1}H NMR chemical shifts of 3a species (δ, ppm in $CDCl_3$).

^{1}H-NMR			^{13}C-NMR			^{1}H-NMR
Atom position	Exp.	Theo.	Atom position	Exp.	Theo.	
Enol						Keto
H17	12.33	12.57	C1	132.92	132.11	18.08
H18	9.36	9.51	C2	134.74	134.21	9.19
H4	7.57	7.89	C3	159.92	160.00	8.23
H6	7.56	7.75	C4	130.77	131.03	8.02
H8	7.56	7.75	C5	121.21	120.96	8.11
H14	7.54	7.60	C6	129.16	129.31	7.64
H16	7.54	7.60	C7	129.16	129.22	7.86
H12	7.50	7.49	C8	128.86	128.74	7.86
H3	7.49	7.42	C9	128.86	128.80	7.76
H5	7.49	7.42	C10	117.53	117.49	7.76
H9	7.28	7.32	C11	129.07	129.00	7.64
H10	7.27	7.23	C12	129.38	129.33	7.53
H19	7.26	7.21	C13	129.38	129.35	7.15
H15	7.07	7.13	C14	131.35	131.37	6.92
H1	7.04	7.04	C15	131.35	131.39	7.37
H7	7.01	6.89	C16	117.20	117.15	7.21
H12	3.60	3.83	C17	145.52	145.45	3.80
H13	3.60	3.72	C18	31.65	30.97	3.80
H11	3.60	3.54	C19	120.17	120.12	3.97
			C20	160.00	161.42	
			C21	129.84	129.79	
			C22	124.8	124.85	
			C23	127.47	127.39	
			C24	130.37	130.35	
			C25	79.46	80.20	

gathered in Table 4 with the experimental values for comparison. The atoms are numbered in Fig. 6.

The DFT-calculated chemical shifts of the Enol tautomer are good in agreement with the experimental values, confirming the suitability of the optimized geometry for the Enol tautomer as the favorite isomer of the titled Schiff base. A signal at about 12.57 ppm is attributed to the phenolic proton, H17 [52]. Unlike to the Enol tautomer, the DFT-chemical shifts of the Keto tautomer are far from the experimental ones. For example, the ^{1}H-NMR chemical shift of the H17 atom predicated to be 18.08 ppm, which is significantly higher than the experimental values. The experimental ^{13}C NMR data exhibited 21 carbons for **3a** which were good in agreement with the theoretical values. For instance, in the experimental spectrum, a signal at about 160.00 ppm was related to the carbon of the phenolic group (C20), which was an agreement with its theoretical value about 161.42 ppm.

NBO analysis

The NBO analysis plays a significant role in the investigation of the intra- and intermolecular bonding interactions and exploring of the charge transfers in chemical compounds [53, 54]. The Enol tautomer of

the species **3a** is more stable than the Keto one. Since the NBO analyses have been performed on the Enol tautomer.

Electron delocalization between donor NBO(*i*) and acceptor NBO(*j*) orbitals causes to the stabilization energy of hyper conjugative interactions (E(2)). Amount of the E(2) is a significant criterion for determining the degree of interaction between electron donor and electron acceptor orbitals. The greater the E(2), the greater the electron transferring tendency from an electron donor to an electron acceptor, resulting in more electron density delocalization, which leads to more stabilization of the system, consequently. The value of E(2) is calculated using

$$E(2) = -q_i \frac{(F_{ij})^2}{\varepsilon_j - \varepsilon_i} \qquad (2)$$

Where q_i, F_{ij}, ε_j, and ε_i parameters are the donor orbital occupancy, the off-diagonal NBO Fock matrix element, energies of the acceptor and donor orbitals, respectively. The lower ε_j-ε_i energy difference results in higher stabilization energy (E(2)). The parameters of Eq.(2) have been obtained from the second-order perturbation theory analysis of Fock matrix in the NBO basis. The selected results for the Enol tautomer of the species **3a** are gathered in Table 5.

As seen, the $\pi \longrightarrow \pi^*$ transitions of the aromatic rings increase the stability of the investigated compound. The NBO interactions imply the existence of a strong O1-H17...N2 hydrogen bond interaction, which stabilizes the compound about 175.35 kJ/mol as the stabilizing energy. The computed charge on the O1, H17 and N2 atoms are -0.71, +0.53 and -0.55, respectively, confirming strong intramolecular H-bond between the N2 and H17 atoms. The strongest interaction inducing the highest stabilization energy is related to the $n(O1) \rightarrow LP^*(H17)$ electron donations.

The 3D-distribution map for the highest-occupied-molecular orbital (HOMO) and the lowest-unoccupied-molecular orbital (LUMO) of the Enol tautomer are shown in Fig. 8. The HOMO orbital is localized on the right side of the molecule, involves the azomethine group. But, the LUMO orbital is localized on the left side of the molecule, mainly on the two phenyl substitutions of the pyrrole ring.

The energy difference between the HOMO and LUMO frontier orbitals is one of the important characteristics of molecules, which plays has an important role in such cases as electric properties, electronic spectra, and photochemical reactions. The value of the energy gap between the HOMO and LUMO orbitals of the Enol tautomer is equal to 3.31eV. This large band gap demonstrates that the species **3a** is stable [55, 56].

The UV-Vis spectrum

The TD-DFT//B3LYP/6-31+G(d,p) calculations were done on the fully optimized ground-state structure of the Enol tautomer to predict its low-lying excited states. The experimental UV-Vis spectrum of the compound **3a** was recorded in DMSO solution. The TD-DFT calculation predicts an intense electronic transition at λ_{max} = 425.5 nm, which is well in agreement with the experimental data (λ_{max}= 425.0 nm) (Fig. 9). This maximum absorbance is corresponding to the electronic transition from the ground state to the first-excited state of the molecule. In other words, it is related to the HOMO $\longrightarrow$ LUMO electron excitation.

CONCLUSIONS

In this work, some new Schiff bases of a pyrrole derivative have been synthesized and characterized using several spectroscopic methods. The fluorescence spectroscopy performed in different solvents, temperatures, and pHs. The results showed the highest fluorescence emission intensity is for DMSO at 15°C and pH = 7.5 for **3a** species. The molecular docking studies revealed that the compound **3a** forms a stable complex with polo-like kinase 1 as a target and gives a binding affinity value of -8.9 kcal/mol.

In addition, the geometry, tautomerism and spectral behavior of a Schiff base **3a** have been computationally investigated employing the DFT approaches. Geometries of the Enol and Keto tautomers as well as kinetics of its tautomerism have been determined theoretically. In methanol solution, the computed electronic and Gibbs free energies show that the Enol tautomer of the species **3a** is more stable than the Keto one. In addition, unlike to the Keto tautomer, the computed ^{1}H-NMR chemical shifts as well as the predicted λ_{max} in UV-Vis spectrum of the Enol tautomerare are in good agreement with

Table 5: The second-order perturbation theory analysis of Fock matrix in NBO basis for Enol tautomer of the 3a

Donor NBO (i)	Acceptor NBO (j)	E_j-E_i(a.u.)[a]	E(2) (kcal/mol)[b]
BD(1) C1-C2	BD*(2) C3-C4	2.32	17.17
BD(2) C3-C4	BD*(2) C1-C2	0.30	19.97
BD(2) C5-C7	BD*(2) C9-C10	0.28	19.92
BD(2) C6-C8	BD*(2) C9-C10	0.28	20.42
BD(2) C9-C10	BD*(2) C5-C7	0.28	20.54
BD(2) C11-C12	BD*(2) C14-C16	0.28	20.24
BD(2) C13-C15	BD*(2) C14-C16	0.28	19.89
BD(2) C14-C16	BD*(2) C11-C12	0.28	20.21
BD(2) C14-C16	BD*(2) C13-C15	0.28	19.93
BD(2) C17-N2	BD*(2) C3-C4	0.35	17.18
BD(2) C19-C21	BD*(2) C17-N2	0.25	24.28
BD(2) C21-C23	BD*(2) C22-C24	0.28	21.89
BD(2) C22-C24	BD*(2) C19-C20	0.27	23.50
LP(1) N1	BD*(2) C3- C4	0.28	44.54
LP(2) O1	BD*(2) C19-C20	0.33	35.14

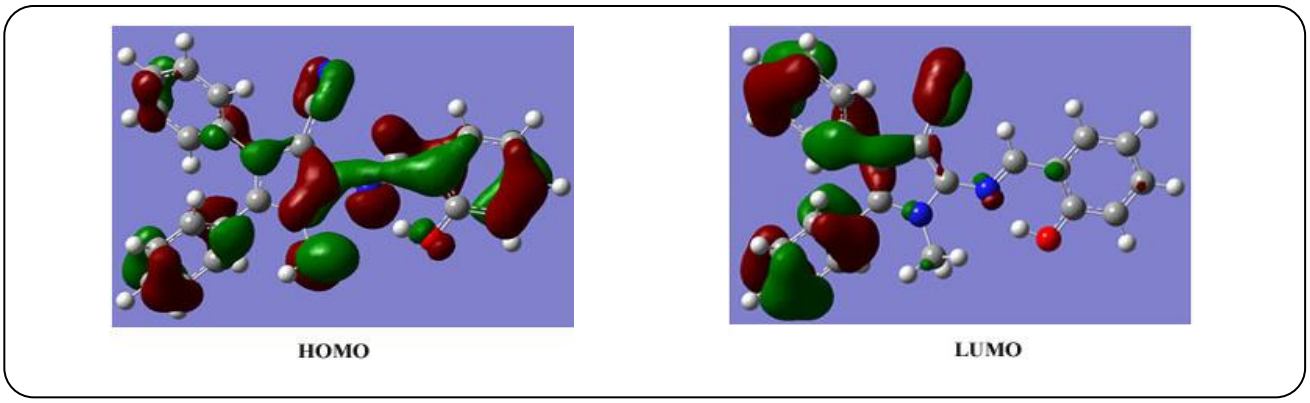

Fig. 8: The HOMO and LUMO frontier orbitals for the Enol tautomer of the species 3a.

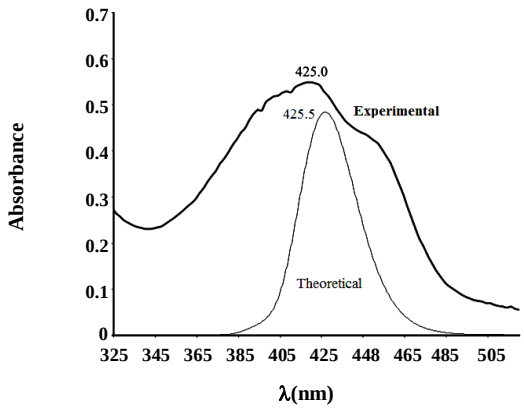

Fig. 9: The experimental and theoretical UV-Vis spectra.

the experimental data. Since the species **3a** could exist as the Enol tautomer. In the optimized geometry of the Enol tautomer, two phenyl moieties lie out of the plane of the molecule. The azomethine group lies in the plane of the benzene ring.

Based on the NBO analysis on the Enol tautomer of the species **3a**, the $\pi \longrightarrow \pi^*$ transitions of the aromatic rings increase the stability of **3a** species. Also, computed stabilization energies and atomic charges indicate strong intramolecular H-bond (O1-H17...N2), which stabilizes the compound considerably. This H-bond affects considerably the ^{1}H-NMR chemical shift of the H17

phenolic proton, too. Shapes of the HOMO-LUMO frontier orbitals have been determined. High energy gap confirms the stability of the species **3a**.

Received : Jun. 9, 2017 ; Accepted : Nov. 20, 2017

REFERENCES

[1] Souzangarzadeh S., 1,3-Dipolar Cycloaddition Reaction of Nitrile Oxides to Isatin Imines, *Iran. J. Chem. Chem. Eng (IJCCE).*, **35**, 31-35 (2016).

[2] Golchoubian H., Nazari O., Soleimani G., Mohseni M., Template Synthesis, Structural Characterization and Antibacterial Activity of an Unsymmetrical Tridentate Schiff Base Nickel(II) Complex, *Iran. J. Chem. Chem. Eng (IJCCE).*, **33**, 65-72 (2014).

[3] Salehi M., Ghasemi F., Kubicki M., Asadi A., Behzad M., Ghasemi M.H., Gholizadeh A., Synthesis, Characterization, Structural Study and Antibacterial Activity of the Schiff Bases Derived from Sulfanilamides and Related Copper(II) Complexes, *Inorg. Chim. Acta.*, **453**: 238-246 (2016).

[4] Parekh N.M., Mistry B.M., Pandurangan M., Shinde S.K., Patel R.V., Investigation of Anticancer Potencies of Newly Generated Schiff Base Imidazolylphenylheterocyclic-2-Ylmethylenethiazole-2-amines, *Chin. Chem. Lett.*, **28**: 602-606 (2017).

[5] Köse M., Ceyhan G., Tümer M., Demirtaş İ., Gönül İ., McKee V., Monodentate Schiff Base Ligands: Their Structural Characterization, Photoluminescence, Anticancer, Electrochemical and Sensor Properties, *Spectrochim. Acta, Part A.*, **137**: 477-485 (2015).

[6] Mondal S., Mandal S.M., Mondal T.K., Sinha C., Spectroscopic Characterization, Antimicrobial Activity, DFT Computation and Docking Studies of Sulfonamide Schiff Bases, *J. Mol. Struct.*, **1127**: 557-567 (2017).

[7] Afzal S., Akhter Z., Gul A., Nadeem M.A., Tahir M.N., Perveen F., Crystal Structure Analysis, Biological Evaluation by Docking and DFT Studies of a Novel Schiff Base, *J. Chem. Soc. Pak.*, **38**: (2016).

[8] Asgharpour Z., Farzaneh F., Abbasi A., Ghiasi M., Synthesis, Crystal Structure and DFT Studies of a New Dioxomolybdenum(VI) Schiff Base Complex as an Olefin Epoxidation Catalyst, *Polyhedron*, **101**: 282-289 (2015).

[9] Judy Azar A.R., Safaei E., Mohebbi S., A Novel Schiff base of Mn(III) Complex supported on Magnetic Cobalt Nanoparticles as a Highly Efficient Retrievable Heterogeneous Catalyst in Oxidation of Alcohols and Sulfides Compounds, *Mater. Res. Bull.*, **70**: 753-761 (2015).

[10] Naeimi A., Saeednia S., Yoosefian M., Rudbari H.A., Nardo V.M., A Novel Dinuclear Shiff Base Copper Complex as an Efficient and Cost Effective Catalyst for Oxidation of Alcohol: Synthesis, Crystal Structure and Theoretical Studies, *J. Chem. Sci.*, **127**: 1321-1328 (2015).

[11] Lakshme S.S., Geetha K., Gayathri M., Shanmugam G., Synthesis, Crystal Structures, Spectroscopic Characterization and in Vitro Antidiabetic Studies of New Schiff Base Copper(II) Complexes, *J. Chem. Sci.*, **128**: 1095-1102 (2016).

[12] Chakraborty J., Singh R.K.B., Samanta B., Choudhury C.R., Dey S.K., Talukder P., Borah M.J., Mitra S., Two New Quadridentate Schiff Base Complexes of Nickel (II) and Cobalt (III): Synthesis, Structure and Spectral Characterisation, *Z. Naturforsch., B: Chem. Sci.*, **61**: 1209-1216 (2006).

[13] Abdel-Rahman L.H., El-Khatib R.M., Nassr L.A., Abu-Dief A.M., Synthesis, Physicochemical Studies, Embryos Toxicity and DNA Interaction of Some New Iron (II) Schiff Base Amino Acid Complexes, *J. Mol. Struct.*, **1040**: 9-18 (2013).

[14] Kumar S., Dhar D.N., Saxena P., Applications of Metal Complexes of Schiff Bases—A Review, *J. Sci. Ind. Res.*, **68**: 181-187 (2009).

[15] Snell E.E., Di Mari S.J., 7 Schiff Base Intermediates in Enzyme Catalysis, *The Enzymes*, **2**: 335-370 (1970).

[16] Nejati K., Rezvani Z., Massoumi B., Syntheses and Investigation of Thermal Properties of Copper Complexes with Azo-containing Schiff-Base Dyes, *Dyes Pigments.*, **75**: 653-657 (2007).

[17] Hart C., Schulenberg B., Steinberg T.H., Leung W.Y., Patton W.F., Detection of Glycoproteins in Polyacrylamide Gels and on Electroblots Using Pro-Q Emerald 488 Dye, a Fluorescent Periodate Schiff-Base Stain, *Electrophoresis*, **24**: 588-598 (2003).

[18] Wang L., Qin W., Liu W., A Sensitive Schiff-base Fluorescent Indicator for the Detection of Zn^{2+}, *Inorg. Chem. Commun.*, **13**: 1122-1125 (2010).

[19] Bellina F., Rossi R., Synthesis and Biological Activity of Pyrrole, Pyrroline and Pyrrolidine Derivatives with Two Aryl Groups on Adjacent Positions, *Tetrahedron*, **62**: 7213-7256 (2006).

[20] Khashi M., Davoodnia A., Lingam V.P.R., DMAP Catalyzed Synthesis of Some New Pyrrolo [3, 2-e] [1, 2, 4] triazolo [1, 5-c] pyrimidines, *Res. Chem. Intermed.*, **41**:5731-5742 (2015).

[21] O'Malley D.P., Li K., Maue M., Zografos A.L., Baran P.S., Total Synthesis of Dimeric Pyrrole-Imidazole Alkaloids: Sceptrin, Ageliferin, Nagelamide E, Oxysceptrin, Nakamuric Acid, and the Axinellamine Carbon Skeleton, *J. Am. Chem. Soc.*, **129**, 4762-4775 (2007).

[22] Kaya İ., Bora E., Aydın A., Synthesis and characterization of Schiff Base Derivative with Pyrrole Ring and Electrochromic Applications of Its Oligomer, *Prog. Org. Coat.*, **77**, 463-472 (2014).

[23] Williams B.M., Barone V., Pate B.D., Peralta J.E., Gradient Copolymers of Thiophene and Pyrrole for Photovoltaics, *Comput. Mat. Sci.*, **96, Part A**, 69-71 (2015).

[24] Choi J.H., Ryu J.Y., Park Y.J., Begum H., Park H.-R., Cho H.J., Kim Y., Lee J., Fluorescent Chemosensor Based on Pyrrole-Aminoindanol for Selective Zinc Detection, *Inorg. Chem. Commun.*, **50**, 24-27 (2014).

[25] Velmathi S., Reena V., Suganya S., Anandan S., Pyrrole Based Schiff Bases as Colorimetric and Fluorescent Chemosensors for Fluoride and Hydroxide Anions, *J. fluoresc.*, **22**, 155-162 (2012).

[26] Tang J., Marcus R., Photoinduced Spectral Diffusion and Diffusion-Controlled Electron Transfer Reactions in Fluorescence Intermittency of Quantum Dots, *J. Chin. Chem. Soc.*, **53**, 1-13 (2006).

[27] Chen M.Y., Hsu M.A., Liu C.Y., Chow T.J., Synthesis and Electroluminescence of Metal 4-Styryl-8-hydroxyquinolates, *J. Chin. Chem. Soc.*, **51**, 735-742 (2004).

[28] Lim T.L., Nazarov M., Yoon T.L., Low L.C., Ahmad Fauzi M.N., X-ray diffraction experiments, luminescence measurements and first-principles GGA + U calculations on YTaO4, *Comput. Mat. Sci.*, **77**, 13-18 (2013).

[29] Yin J., Lu X., Dong Q., First Principles Study the Luminescence Mechanism of Wurtzite $AgInS_2$ Doped by Zinc, *Comput. Mat. Sci.*, **122**: 86-91 (2016).

[30] Kim K.B., Kim H., Song E.J., Kim S., Noh I., Kim C., A Cap-type Schiff Base Acting as a Fluorescence Sensor for Zinc (II) and a Colorimetric Sensor for Iron (II), Copper (II), and Zinc (II) in Aqueous Media, *Dalton Transactions*, **42**: 16569-16577 (2013).

[31] Lee S.A., You G.R., Choi Y.W., Jo H.Y., Kim A.R., Noh I., Kim S.-J., Kim Y., Kim C., A New Multifunctional Schiff Base as a Fluorescence Sensor for Al^{3+} and a Colorimetric Sensor for CN- in Aqueous Media: an Application to Bioimaging, *Dalton Trans.*, **43**: 6650-6659 (2014).

[32] Yang L., Zhu W., Fang M., Zhang Q., Li C., A new Carbazole-Based Schiff-Base as Fluorescent Chemosensor for Selective Detection of Fe^{3+} and Cu^{2+}, *Spectrochim. Acta, Part A.*, **109**: 186-192 (2013).

[33] Bavadi M., Niknam Kh., Shahraki O., Novel Pyrrole Derivatives Bearing Sulfonamide Groups: Synthesis in Vitro Cytotoxicity Evaluation, Molecular Docking and DFT Study, *J. Mol. Struct.*, **1146**: 242-253 (2017).

[34] Mohajeri S., Noei M., Molaei N., Cyanogen, Methylacetylene, Hydroquinone, Ethylacetylene, Aniline, Pyrrole, and Ethanol detection by using BNNT: DFT Studies, *Iran. J. Chem. Chem. Eng. (IJCCE).*, (2017) in press.

[35] Bandyopadhyay D., Layek M., Fleck M., Saha R., Rizzoli C., Synthesis, Crystal Structure and Antibacterial Activity of Azido Complexes of Cobalt(III) Containing Heteroaromatic Schiff Bases, *Inorg. Chim. Acta.*, **461**: 174-182 (2017).

[36] Ghorab M.M., Ragab F.A., Heiba H.I., Youssef H.A., El-Gazzar M.G., Synthesis of Novel Pyrazole and Pyrimidine Derivatives Bearing Sulfonamide Moiety as Antitumor and Radiosensitizing Agents, *Med. Chem. Res.*, **21**: 1376-1383 (2012).

[37] Tomašič T., Mirt M., Barančoková M., Ilaš J., Zidar N., Tammela P., Kikelj D., Design, Synthesis and Biological Evaluation of 4,5-dibromo-N-(thiazol-2-yl)-1H-pyrrole-2-carboxamide Derivatives as Novel DNA Gyrase Inhibitors, *Biorg. Med. Chem.*, **25**: 338-349 (2017).

[38] Downward J., Finding the Weakness in Cancer, *N. Engl. J. Med.*, **361**, 922-924 (2009).

[39] Luo J., Emanuele M.J., Li D., Creighton C.J., Schlabach M.R., Westbrook T.F., Wong K.-K., Elledge S.J., A Genome-Wide RNAi Screen Identifies Multiple Synthetic Lethal Interactions with the Ras Oncogene, *Cell*, **137**: 835-848 (2009).

[40] Valeur B., Berberan-Santos M.N., "Molecular Fluorescence: Principles and Applications", John Wiley & Sons, Inc., (2012).

[41] Skoog D.A., West D.M., "Principles of Instrumental Analysis", Saunders College Philadelphia, (1980).

[42] Lakowicz J.R., "Principles of Fluorescence Spectroscopy", Springer Science & Business Media, (2013).

[43] White A., Effect of pH on Fluorescence of Tyrosine, Tryptophan and Related Compounds, *Biochem. J.*, **71**: 217- (1959).

[44] Trott O., Olson A.J., AutoDock Vina: Improving the Speed and Accuracy of Docking with a New Scoring Function, Efficient Optimization, and Multithreading, *J. Comput. Chem.*, **31**, 455-461 (2010).

[45] Frisch M., Trucks G., Schlegel H., Scuseria G., Robb M., Cheeseman J., Montgomery Jr J., Vreven T., Kudin K., Burant J., Gaussian 03, Revision B. 05; Gaussian, Inc., Pittsburgh, PA, 12478 (2003).

[46] Young D.C., "Computational Chemistry: A Practical Guide for Applying Techniques to Real World Problems", 42 (2004).

[47] Ditchfield R., Self-Consistent Perturbation Theory of Diamagnetism: I. A Gauge-Invariant LCAO Method for NMR Chemical Shifts, *Mol. Phys*, **27**: 789-807 (1974).

[48] Beyramabadi S., Morsali A., Shams A., N, N′-Dipyridoxyl (1, 2-diaminocyclohexane) and Its Cu (II) Complex: Synthesis, Experimental and Theoretical Studies, *J. Struct. Chem.*, **56**: 243-249 (2015).

[49] Khashi M., Beyramabadi S.A., Davoodnia A., Ettehadi Z., Synthesis, Experimental and Theoretical Characterizations of Some New Pyrrolo [2, 3-d] pyrimidine Derivatives Bearing an Aromatic Sulfonamide Moiety, *J. Mol. Struct.*, (2017).

[50] Habibi M., Beyramabadi S.A., Allameh S., Khashi M., Morsali A., Pordel M., Khorsandi-Chenarboo M., Synthesis, Experimental and Theoretical Characterizations of a new Schiff Base Derived from 2-Pyridincarboxaldehyde and Its Ni (II) Complex, *J. Mol. Struct.*, **1143**: 424-430 (2017).

[51] Toozandejani T., Beyramabadi S.A., Chegini H., Khashi M., Morsali A., Pordel M., Synthesis, Experimental and Theoretical Characterization of a Mn (II) Complex of N, N′-dipyridoxyl (1, 2-diaminobenzene), *J. Mol. Struct.*, **1127**: 15-22 (2017).

[52] Dal H., Süzen Y., Şahin E., Synthesis, Spectral Studies of Salicylidine-Pyridines: Crystal and Molecular Structure of 2-[(1E)-2-aza-2-(5-methyl (2-pyridyl) ethenyl)]-4-bromobenzen-1-ol, *Spectrochim. Acta, Part A*, **67**: 808-814 (2007).

[53] Schwenke D.W., Truhlar D.G., Systematic Study of Basis Set Superposition Errors in the Calculated Interaction Energy of Two HF Molecules, *J. Chem. Phys.*, **82**: 2418-2426 (1985).

[54] Tezer N., Karakus N., Theoretical Study on the Ground State Intramolecular Proton Transfer (IPT) and Solvation Effect in Two Schiff Bases Formed by 2-aminopyridine with 2-hydroxy-1-naphthaldehyde and 2-hydroxy Salicylaldehyde, *J. Mol. Model.*, **15**: 223-232 (2009).

[55] Snehalatha M., Ravikumar C., Joe I.H., Sekar N., Jayakumar V., Spectroscopic Analysis and DFT Calculations of a Food Additive Carmoisine, *Spectrochim. Acta, Part A*, **72**: 654-662 (2009).

[56] Sadeghzade Z., Beyramabadi S.A., Morsali A., A DFT Investigation of Structure, Spectroscopic Properties and Tautomerism of the Anticonvulsant Drug Lyrica, *Spectrochim. Acta, Part A*, **138**: 637-642 (2015).